

Short Communication

Carbon Encapsulated WS₂ Nanocomposites Derived from ZIF-67@WS₂ Core-Shell Nanoparticles and their electrocatalytic applications

Qijian Niu^{1,3}, Oluwafunmilola Ola³, Nannan Wang^{2,3,*}, Binling Chen^{3,*}, Yanqiu Zhu³, Yongde Xia³

¹ School of Agricultural Engineering, Jiangsu University, Zhenjiang, Jiangsu, 212013, China

² Guangxi institute for Fullerene Technology, Key Laboratory of New Processing Technology for Nonferrous Metals and Materials, School of Resources Environment and Materials, University of Guangxi, Nanning, Guangxi, 530000, China

³ College of Engineering, Mathematics and Physical Sciences, University of Exeter, Exeter, EX4 4QF, UK

*E-mail: wangnannan@gxu.edu.cn ; B.Chen@exeter.ac.uk

Received: 29 August 2020 / Accepted: 20 October 2020 / Published: 31 October 2020

In this work, Co₉S₈ and N,S co-doped carbon encapsulated WS₂ nanocomposites (Co₉S₈-N,S-C@WS₂) has been successfully prepared through a high-temperature carbonization of the precursor ZIF-67@WS₂ nanoparticles. The obtained Co₉S₈-N,S-C@WS₂ nanoparticles were confirmed to have a core-shell structure and uniform element distribution by TEM and element mapping. Its crystal structure was characterized by XRD, and the high specific surface areas with porous structure was characterized by BET tests. The as-prepared Co₉S₈-N,S-C@WS₂ nanoparticles exhibited a better ORR/OER/HER performance than single component. In this work, a novel idea for the preparation of functional nanocomposite materials could be provided.

Keywords: WS₂, ZIF-67, core-shell nanoparticles, electrocatalysts

1. INTRODUCTION

Nanomaterials have received extensive researches and attentions from scientists due to their excellent physical and chemical properties. Among them, the core-shell nanoparticles have been used in different fields, such as energy[1], environmental[2], medicine[3], electronics[4] sensors[5] and so on. Recently, the use of MOFs in situ growth to construct core-shell structures has been widely studied[6]. Bai et al. prepared a Si@ZIF-67 composites by a simple liquid phase method. This composites had been used as an anode material in a lithium-ion battery[7]. Guo et al. reported a novel double core-shell structured CNH@PDA@NiMOFs (CNH-D-NiMOFs) composite based on the support of carbon

nanohorns (CNHs) and the direction of polydopamine (PDA) on the synthesis of metal-organic frameworks (MOFs). It was found that this unique structure could improve the electrocatalytic performance and stability of the composites[8]. Lü et al. reported a strategy to prepare a highly dispersed Co-embedded porous carbon nanocage (CoPCN) structure derived from a core-shell ZIF-8@ZIF-67 precursor. High Co loading (over 30 wt %) can be achieved while maintaining an optimal dispersion and particle size of the active Co phase when a ZIF-8@ZIF-67 is pyrolyzed at 920°C[9]. Through the high-temperature carbonization of MOFs composites, the construction of functional nanomaterials can be realized, especially the transition metal-doped carbon nanocomposites[10]. WS₂ is a metal sulfide with excellent properties. It also has been widely used in energy[11], environment[12], medicine[13], sensing[14] and other fields. Therefore, it is of great significance to construct its composite materials. At present, the construction of core-shell composite materials by in-situ growing MOFs on the surface of WS₂ is rarely reported.

In this work, a novel ZIF-67@WS₂ core-shell nanoparticles were first prepared by a simple in situ growth method. The core-shell Co₉S₈-N,S-C@WS₂ composites were then prepared by a high-temperature carbonization of ZIF-67@WS₂ core-shell nanoparticles. The core-shell structure of Co₉S₈-N,S-C@WS₂ were characterized by TEM and element mapping. Its crystal structure and composition was characterized by XRD. The as-prepared Co₉S₈-N,S-C@WS₂ exhibited improved electrocatalytic performance comparing to the pure WS₂ and ZIF-67 carbide products. This core-shell structure preparation method can provide a novel ideas for the design of new electrocatalytic materials.

2. EXPERIMENTAL SECTION

2.1 The preparation of ZIF-67@WS₂ and Co₉S₈-N,S-C@WS₂

The WS₂ nanoparticles was prepared using as-reported method[15]. After that, the ZIF-67@WS₂ nanoparticles was produced by a simple method: 100 mg WS₂ nanoparticles was dispersed into 30 mL deionized water under ultrasonic state; then, 145.5 mg Co(NO₃)₂·6H₂O (from Aladdin Industrial Corporation) was added into the solution for adsorption 30 min; After that, 10 mL containing 492.0 mg 2-Methylimidazole (MIM, from Aladdin Industrial Corporation) aqueous solution was added for continuous 3 h reaction. At last, centrifuge the sample and wash it with deionized water three times, then dry it in vacuum oven for later use. The carbonization process was carried out in the vacuum tube furnace. The temperature was raised to the different target temperatures (600, 800, and 1000°C) with a heating rate of 10 °C/min and kept for 2 h in Ar atmosphere, then lowered to room temperature to obtain the final carbonization samples.

2.2 Materials characterization

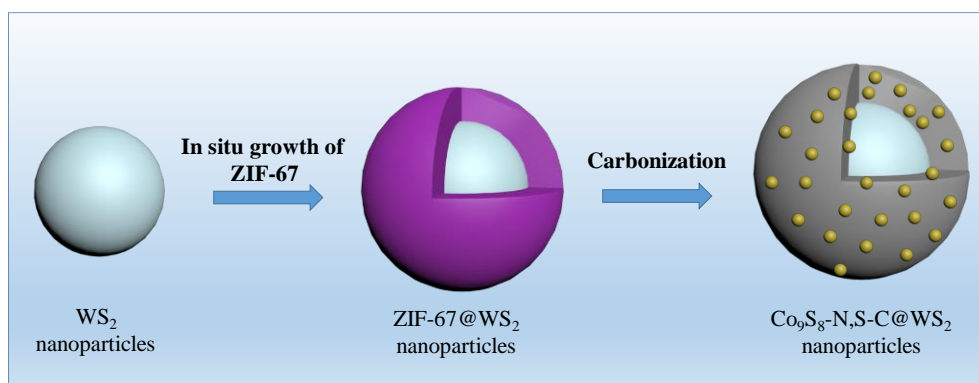
Transmission electron microscopy (TEM, JOEL-2100) was used to characterize its microstructure and selected area electron diffraction (SAED) was selected to characterize its crystal characteristics. The element distribution and linear scan (STEM image and linear EDX) represent the

element distribution. Brunauer-Emmett-Teller (BET, Quantachrome Autosorb-iQ gas sorptometer) was used to characterize the specific surface area of the samples[16].

2.3 Electrochemical characterization

The electrochemical tests were performed using a conventional three-electrode system. The electrochemical workstation is CHI-760D coupled with a rotating disk electrode (RDE) system. The counter electrode is a Pt wire, the reference electrode is a Ag/AgCl/KCl (saturated solution). The bare modified glassy carbon electrode (GCE) with 3.0 mm diameter is the working electrode. The 0.1 M KOH, 1.0 M KOH and 0.5 M H₂SO₄ solutions were used as electrolyte for ORR, OER, and HER tests respectively. Before ORR and OER testing, the O₂ was pumped into electrolyte for 30 min to saturate it. To prepare catalyst ink, 3.0 mg catalyst was dispersed into 1.0 mL of water/ethanol (v/v=4:1) solution with additional 5.0 uL of 5 wt% nafion solution by ultrasonic for 30 min. The 5.0 uL catalyst ink was deposited onto the working electrode and dry naturally. Linear sweep voltammetric curves (LSV) were tested at 1600 rpm with a sweep rate of 10 mV s⁻¹ after 50 cycles stabilization of cyclic voltammetry[17].

3. RESULTS AND DISCUSSION



Scheme 1. The preparation process of ZIF-67@WS₂ and Co₉S₈-N,S-C@WS₂ nanocomposites.

The preparation process of ZIF-67@WS₂ and Co₉S₈-N,S-C@WS₂ nanocomposites is shown in Scheme. 1, which consists of in situ crystal growth and high temperature carbonization process. The TEM images were used to characterize core-shell structure of the composite nanoparticles. The selective area electron diffraction (SAED) patterns were selected to characterize their crystallinity (Fig. 1). From Fig. 1a, the WS₂ nanoparticles have a spherical structure similar to cabbage. Its SAED pattern showed strong concentric diffraction rings, indicating good crystalline properties. In Fig. 1b, ZIF-67@WS₂ nanoparticles have a complete core-shell structure.

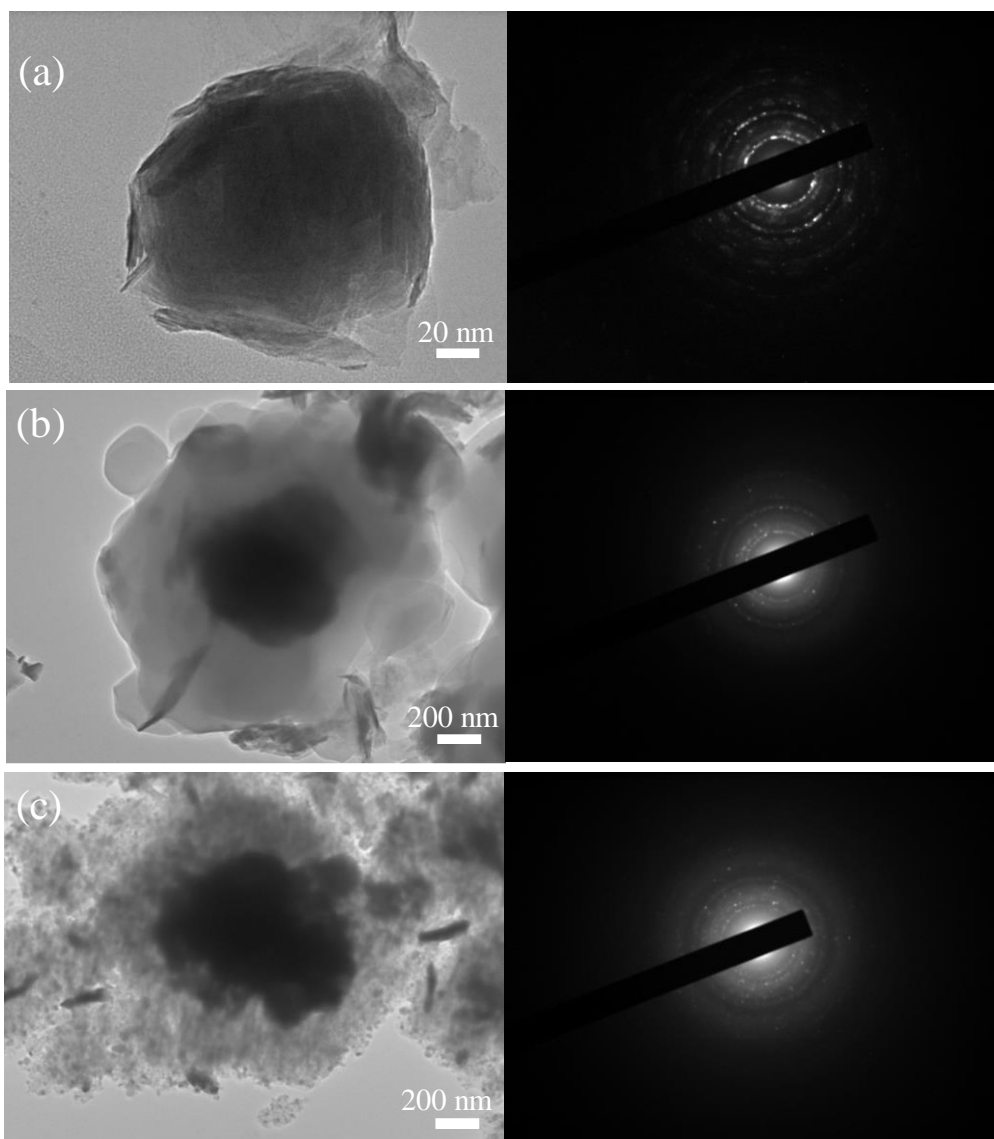


Figure 1. The TEM images of different samples: (a) WS₂ ; (b) ZIF-67@WS₂; and (c) Co₉S₈-N,S-C@WS₂ nanoparticles.

The shell layer is the ZIF-67 nanocrystals and the core layer is original WS₂ nanocrystals. Its SAED pattern showed weaker diffraction rings, due to the coverage of ZIF-67 crystals on the surface of WS₂ core. In Fig. 1c, the core-shell structure can be remained after high temperature carbonization. Meanwhile, it is obvious that many tiny nanoparticles were generated and embedded into the shell layer. Its SAED pattern showed more diffraction spots, corresponding to the nanoparticles formed from the decomposition of ZIF-67[18].

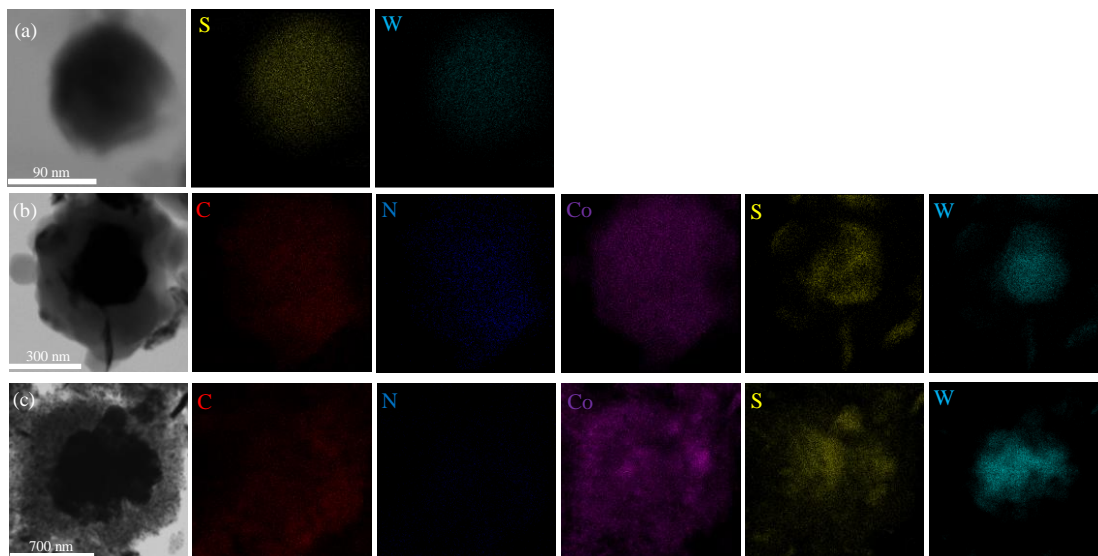


Figure 2. The surface scanning elemental mapping of different samples: (a) WS₂ ; (b) ZIF-67@WS₂; and (c) Co₉S₈-N,S-C@WS₂ nanoparticles.

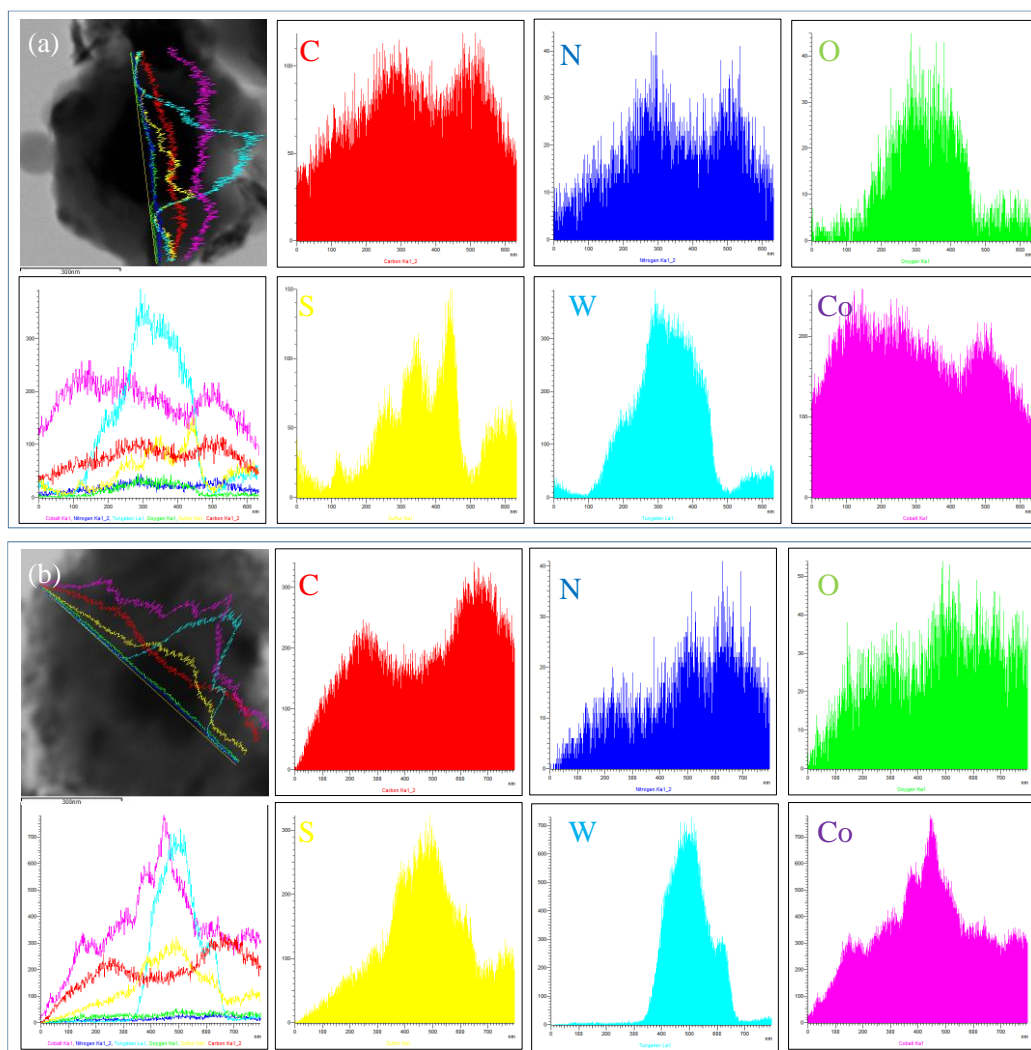


Figure 3. The line scan elemental mapping of different samples: (a) ZIF-67@WS₂; and (b) Co₉S₈-N,S-C@WS₂ nanoparticles.

For further to observe the core-shell structure and the each element distribution more intuitively, the surface scanning elemental mapping of different samples were carried out. From Fig. 2a, it can be seen that only S and W elements exist in pure WS₂ nanoparticles, while in Fig. 2b and Fig. 2c, the C, N, and Co elements were observed except from S and W elements. The C, N, and Co elements came from ZIF-67 and its carbonized derivatives. Obviously, the S and W elements are still mainly distributed in the core layer of the nanoparticles, which intuitively demonstrates the formation of core-shell structure. The difference between Fig. 2b and Fig. 2c is the increasing distribution area of S element. It could be due to that partial WS₂ from the core decomposed during the carbonization process, leading to the doping of S element into the shell layer.

The line scan elemental mapping was also carried out to investigate the element distribution. The same results are obtained that S and W elements are mainly distributed in the core nanoparticles, the C, N, S, and Co elements can be observed in the shell layer. In addition, it was found that during the carbonization, Co element was diffused into the core layer in the as-prepared Co₉S₈-N,S-C@WS₂ nanocomposites.

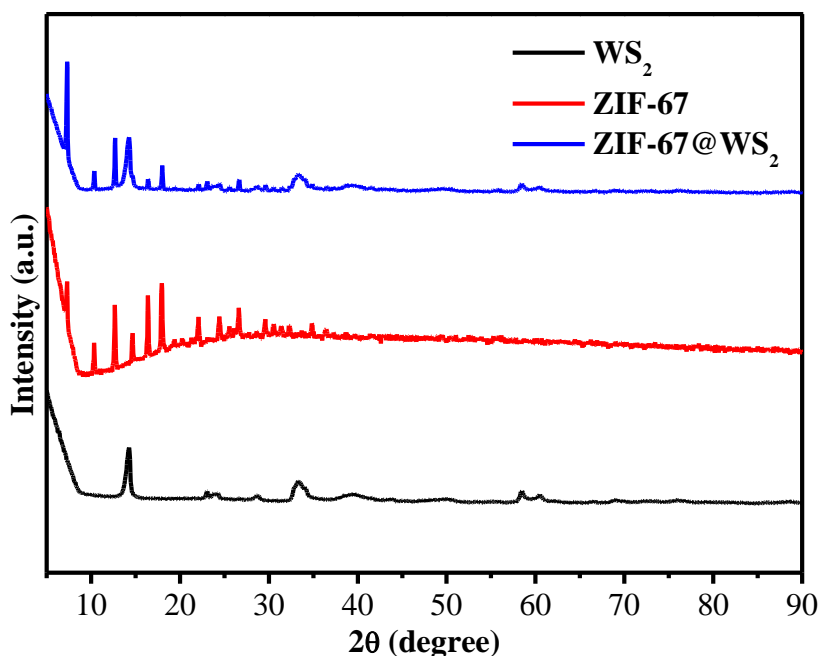


Figure 4. The XRD patterns of different samples: WS₂; ZIF-67; and ZIF-67@WS₂ nanoparticles.

The crystal structures of different samples were tested by the XRD patterns. As shown in Fig. 4, it can be seen that the pure WS₂ nanoparticles has peaks at 14.437°, 33.484°, 58.722°, and 60.545°, corresponding to the WS₂ (003) (101) (110) (1010) crystal surface, respectively (PDF no. 35-0651). The as-prepared ZIF-67 XRD pattern is in consistent with the literature[19]. The ZIF-67@WS₂ XRD pattern combined the peaks of ZIF-67 and WS₂, indicating that the ZIF-67@WS₂ nanocomposites were made successfully.

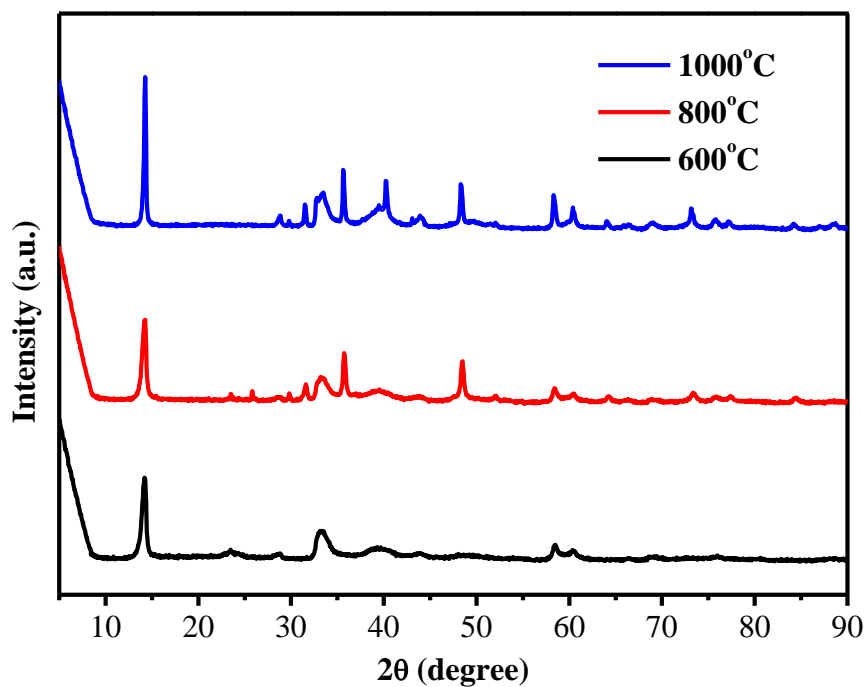


Figure 5. The XRD patterns of different samples at various carbonization temperatures: 600°C; 800°C; and 1000°C.

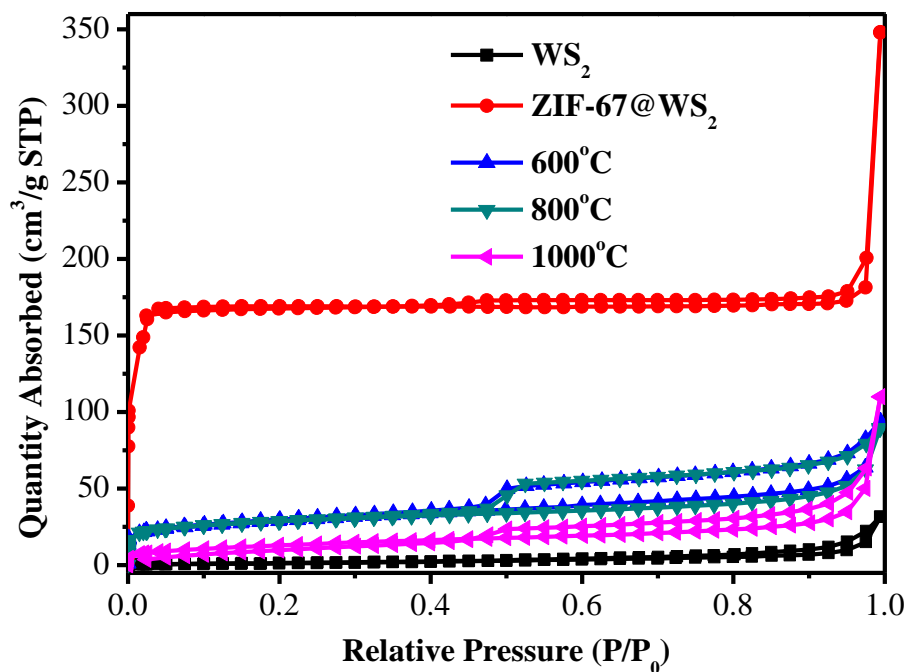


Figure 6. The BET spectra of different samples and different samples at various carbonization temperatures: WS₂; ZIF-67; 600°C; 800°C; and 1000°C.

The crystal structures of various samples at different carbonization temperatures were characterized by the XRD patterns. As shown in Fig. 5, no obvious change was found in 600°C, only the peaks of WS₂ crystal. When the carbonization temperature is above 600°C, two new peaks appeared at 36.190°, 47.568° corresponding to Co₉S₈ (400) and (511) crystal surface, respectively (PDF no. 02-1459). The results suggested that Co₉S₈ was formed by the volatile Co and S elements from the decomposition of ZIF-67 and WS₂ nanocrystals. Meanwhile, with increase of the carbonization temperature, the crystallization of WS₂ is also obviously enhanced.

The BET tests of different samples were also measured. As can be seen in Fig. 6, the WS₂ nanoparticles has the lowest specific surface area of 6.031 m²/g. The core-shell nanoparticles of ZIF-67@WS₂ has the highest specific surface area of 568.529 m²/g, this is mainly due to the porous structure of ZIF-67[20]. With increase of the carbonization temperature, the specific surface area first increases from 100.702 m²/g and then decreases to 47.823 m²/g, which is caused by the collapse of the crystal structure during carbonization[21]. Meanwhile, after carbonization, obvious hysteric structures appeared, which proved the formation of mesoporous structures. These mesoporous structures are very important in the construction of active points in electrochemical catalysis, which is conducive to the improvement of catalytic performance.

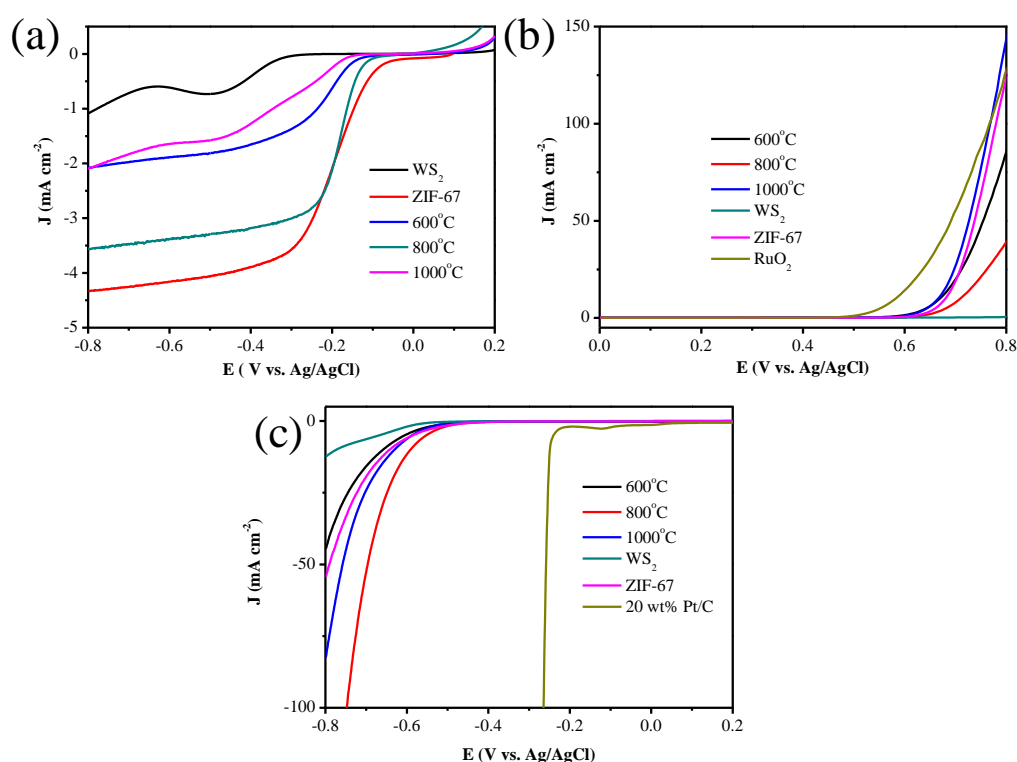


Figure 7. The various electrochemical performances of different samples: LSV curves of (a) ORR in 0.1 M KOH; (b) OER in 1.0 M KOH; (c) HER in 0.5 M H₂SO₄ electrolyte.

The applications of oxygen reduction reaction (ORR), oxygen evolution reaction (OER) and hydrogen evolution reaction (HER) in the energy field were further explored (Fig. 7). As shown in Fig.

7a, the pure WS₂ has poor ORR performance, the performance is greatly improved after forming the composite materials, and the performance is the best at 800°C, where the current density reached -0.1 mA cm⁻², the on-set potential is -0.105 V (Ag/AgCl) and half wave potential is -0.192 V for ORR. However, its performance is still lower than that of the carbonized ZIF-67, which is due to the lack of good synergistic effect. As shown in Fig. 7b, it exhibits superior performance over individual components at the carbonization temperature of 1000°C for OER, the potential is 0.667 V when the current density is equal to 10 mA cm⁻², which possibly due to the production of small amounts of Co₉S₈ and the porous structure. Co₉S₈ is a very good OER catalyst and the porous structure facilitates the material transfer in the catalytic process[22]. As shown in Fig. 7c, it shows the best HER performance, when the carbonization temperature is 800°C. Although the performance is worse than 20 wt% Pt/C, it is better than WS₂ and ZIF-67 carbide products[23]. Although the performance of ORR, OER, and HER are lower than that of commercial catalysts and still needs to be improved, the core-shell structure is better than that of a single component, which indicates that the core-shell structure is still useful. This new composite preparation method provides a possibility for its application in the energy field.

4. CONCLUSION

In conclusion, the ZIF-67@WS₂ core-shell nanoparticles were prepared by a simple in situ growth method. Then, the core-shell Co₉S₈-N,S-C@WS₂ composites were further prepared by high-temperature carbonization and their electrocatalytic properties about ORR, OER, and HER were studied. It was found the core-shell structure can improve the electrocatalytic performance. The core-shell structure of ZIF-67@WS₂ and Co₉S₈-N,S-C@WS₂ were characterized by TEM and element mapping. Their crystal structure and composition was characterized by XRD. The functional composite nanoparticles show some electrochemical properties, which can provide novel ideas for the design and preparation of new nanomaterials and their applications in energy field.

ACKNOWLEDGEMENTS

This work was supported by the China Postdoctoral Science Foundation (Grant no. 2020M671359) and Natural Science Foundation of Jiangsu Province (Grant no.BK20200914)

References

1. S.M. Zhang, J.W. Wu, J.T. Wang, W.M. Qiao, D.H. Long, and L.C. Ling, *J. Power Sources*, 396 (2018) 88.
2. Y.T. Xu, B.L. Chen, J. Nie, and G.P. Ma, *Appl. Surf. Sci.*, 495 (2019) 143577.
3. Y.Y. Hu, Y.R. Liu, X.Y. Xie, W.D. Bao, and J.C. Hao, *J. Colloid Interface Sci.*, 529 (2018) 547.
4. W. Feng, Y.M. Wang, Y.C. Zou, J.C. Chen, D.C. Jia, and Y. Zhou, *Chem. Eng. J.*, 342 (2018) 364.
5. G.J. Ren, Z.M. Li, W.T. Yang, M. Faheem, J.B. Xing, X.Q. Zou, Q.H. Pan, G.S. Zhu, and Y. Du, *Sensor Actuat B-Chem*, 284 (2019) 427.
6. Y.L. Liu and Z.Y. Tang, *Adv. Mater.*, 25 (2013) 5819.
7. Y. Bai, M. Zeng, X. Wu, Y.Q. Zhang, J.W. Wen, and J. Li, *Appl. Surf. Sci.*, 510 (2020) 145477.

8. Y.L. Guo, Y. Zhou, Y.L. Nan, B. Li, and X.L. Song, *ACS Appl. Mater. Interfaces*, 12 (2020) 12743.
9. B.Z. Lü, W.J. Qi, M.S. Luo, Q.L. Liu, and L. Guo, *Ind Eng Chem Res*, 59 (2020) 12352.
10. H.F. Wang, L.Y. Chen, H. Pang, S. Kaskel, and Q. Xu, *Chem. Soc. Rev.*, 49 (2020) 1414.
11. M. Schenato, C.L. Azanza Ricardo, P. Scardi, R. Edla, A. Miotello, M. Orlandi, and R. Morrish, *Appl. Catal., A*, 510 (2016) 156.
12. L. Wang, K.M. Wang, R.H. Huang, Z. Qin, Y.C. Su, and S.S. Tong, *Chemosphere*, 252 (2020) 126578.
13. Y.B. Liu, and J.W. Liu, *Nanoscale*, 9 (2017) 13187.
14. P.Y. Wang, A.C. Wang, M.M. Hassan, Q. Ouyang, H.H. Li, and Q.S. Chen, *Sensor Actuat B-Chem*, 320 (2020) 128434.
15. F. Xu, T.P. Almeida, H. Chang, Y.D. Xia, M.L. Wears and Y.Q. Zhu, *Nanoscale*, 5 (2013) 10504.
16. Q.J. Niu, O. Ola, B.L. Chen, Y.Q. Zhu, Y.D. Xia, and G.P. Ma, *Int. J. Electrochem. Sci.*, 15 (2020) 4869.
17. Q.J. Niu, B.L. Chen, J.X. Guo, J. Nie, X.D. Guo, and G.P. Ma, *Nano-Micro Lett.*, 11(2019) 8.
18. B.L. Chen, R. Li, G.P. Ma, X.L. Gou, Y.Q. Zhu and Y.D. Xia, *Nanoscale*, 7 (2015) 20674.
19. K. Zhou, B. Mousavi, Z.X. Luo, S. Phatanasri, S. Verpoort, and F. Chaemchuen, *J. Mater. Chem. A*, 5 (2017) 952.
20. J.F. Qian, F. Sun, and L.Z. Qin, *Mater. Lett.*, 82 (2012) 220.
21. Q.J. Niu, J.X. Guo, B.L. Chen, J. Nie, X.D. Guo, and G.P. Ma, *Carbon*, 114 (2017) 250.
22. B.L. Chen, G.P. Ma, Y.Q. Zhu, J.B. Wang, W. Xiong, and Y.D. Xia, *J. Power Sources*, 334 (2016) 112.
23. Z. Huang, Z.X. Yang, M.Z. Hussain, B.L. Chen, Q.L. Jia, Y.Q. Zhu, Y.D. Xia, *Electrochim Acta*, 330 (2020) 135335.

© 2020 The Authors. Published by ESG (www.electrochemsci.org). This article is an open access article distributed under the terms and conditions of the Creative Commons Attribution license (<http://creativecommons.org/licenses/by/4.0/>).